1 **Activation of proneuronal transcription factor *Ascl1* in maternal liver ensures a**

2 **healthy pregnancy**

3

4 Joonyong Lee[1], Veronica Garcia[1], Shashank M. Nambiar[1], Huaizhou Jiang[1], and Guoli

5 Dai[1]

6

7 [1]Department of Biology, School of Science, Indiana University-Purdue University

8 Indianapolis, Indianapolis, IN 46202

9

Authors' email

11 Joonyong Lee, PhD, Email: lee224@iu.edu; Veronica Garcia, Email: garciave@iu.edu;

12 Shashank M. Nambiar, Email: snambiar@iu.edu; Huaizhou Jiang, PhD, Email:

13 huajiang@iu.edu; and Guoli Dai, DVM, PhD, Email: gdai@iupui.edu.

14

Corresponding author

16 Guoli Dai, DVM, PhD; 723 West Michigan Street, SL306. Indianapolis, IN 46202; Tel:

17 913-709-2906; Email: gdai@iupui.edu.

18

23

24

Conflict of interest

26 No conflicts of interest, financial or otherwise, are declared by the authors.

27

Author contributions

29 Conceptualization: JL and GD. Investigation: JL, VG, SN, and HJ. Formal analysis: JL,

30 VG, and HJ. Data curation: JL, VG, and HJ. Writing: JL and GD. Resources: GD.

31

Abbreviations

33 Ascl1, achaete-scute homolog-like 1; IGF2, insulin-like growth factor 2; AST, aspartate

34 aminotransferase; ALT, alanine aminotransferase; PL, placental lactogen; GD, gestation

35 day.

36

37 **Main text word count:** 4,908 words including introduction, materials and methods,

38 results, and discussion.

39

40

Synopsis

42

How the maternal liver adapts to pregnancy remains elusive. We found that maternal

liver activates the expression of *Ascl1*, a gene encoding a proneuronal transcription

factor, to coordinate the adaptations of maternal organs and the growth of the placenta,

enabling a healthy pregnancy and normal postnatal growth of the offspring.
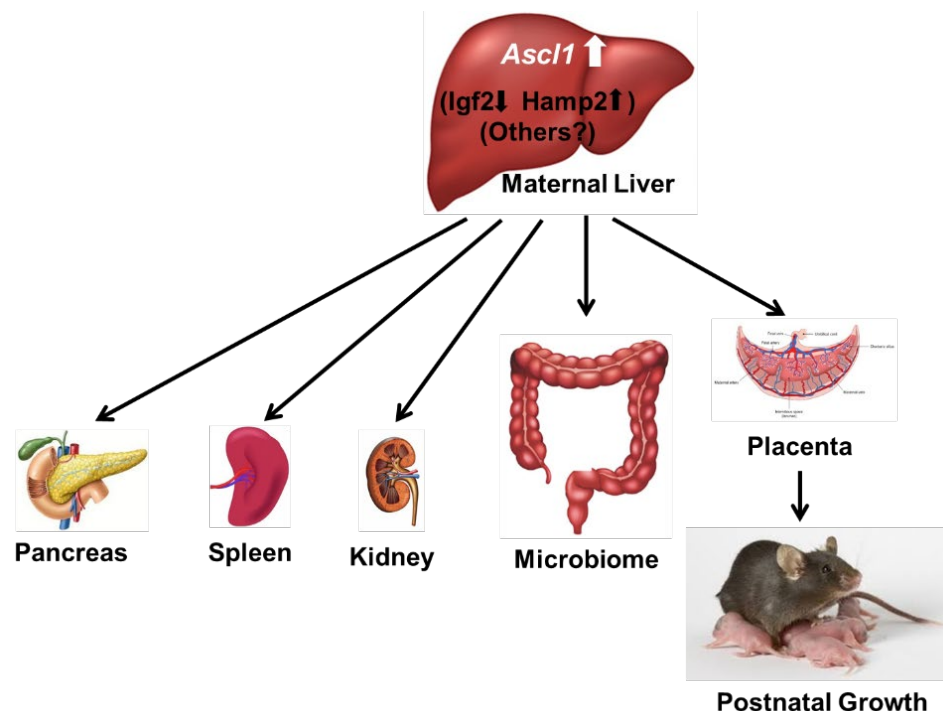
47

Abstract

49

Background & Aims: Maternal liver exhibits robust adaptations to pregnancy to

accommodate the metabolic needs of developing and growing placenta and fetus by

largely unknown mechanisms. We found that achaete-scute homolog-like 1 (*Ascl1*), a

basic helix-loop-helix transcription factor essential for neuronal development, is highly

activated in maternal hepatocytes during the second half of gestation in mice. **Methods:**

To investigate whether and how *Ascl1* plays a pregnancy-dependent role, we deleted

the *Ascl1* gene specifically in maternal hepatocytes from mid-gestation until term.

Results: As a result, we identified multiple *Ascl1*-dependent phenotypes. Maternal

livers lacking *Ascl1* exhibited aberrant hepatocyte structure, increased hepatocyte

proliferation, enlarged hepatocyte size, reduced albumin production, and elevated

release of liver enzymes, indicating maternal liver dysfunction. Simultaneously, maternal

pancreas and spleen and the placenta displayed marked overgrowth; and the maternal

ceca microbiome showed alterations in relative abundance of several bacterial

63   subpopulations. Moreover, litters born from maternal hepatic *Ascl1*-deficient dams

64   experienced abnormal postnatal growth after weaning, implying an adverse pregnancy

65   outcome. Mechanistically, we found that maternal hepatocytes deficient for *Ascl1*

66   exhibited robust activation of *insulin-like growth factor 2* expression, which may

67   contribute to the *Ascl1*-dependent phenotypes widespread in maternal and

68   uteroplacental compartments. **Conclusion:** In summary, we demonstrate that maternal

69   liver, via activating *Ascl1* expression, modulates the adaptations of maternal organs and

70   the growth of the placenta to maintain a healthy pregnancy. Our studies reveal *Ascl1* as

71   a novel and critical regulator of the physiology of pregnancy.

72

73   **Keywords**

74   *Ascl1*, hepatocyte, liver, pregnancy, insulin-like growth factor 2

75

76

77

78

79

80

81

82

83

84

85

86

87

Graphical Abstract

88

89

Introduction

91

The establishment and maintenance of pregnancy requires highly coordinated

adaptations in maternal, uteroplacental, and fetal compartments. As pregnancy

progresses, in the maternal compartment, the liver grows to expand its metabolic

capacity; the pancreas proliferates its β-cell population to elevate insulin production; the

gut alters its microbiome contributing to immunological adjustments; the spleen

undergoes development and growth of the erythroid lineage; and the kidney expands its

volume allowing for increases in blood flow and fluid retention [1-6]. These adaptations of

maternal non-reproductive organs to pregnancy must be required to suffice the

100   demands of the developing and growing placenta and fetus. However, the physiological

101   significance and the regulatory mechanisms of these processes are poorly understood,

102   representing an emerging research field.

103

104   Our work and that of others have demonstrated that maternal liver undergoes

105   hyperplasia and hypertrophy, changes its gene expression profile, and thereby

106   markedly expands during gestation in rodents [7-9]. However, how this is controlled

107   remains elusive. We previously showed that achaete-scute homolog-like 1 (*Ascl1*), a

108   basic helix-loop-helix transcription factor essential for neurogenesis [10-12], is highly

109   upregulated in maternal livers of pregnant rats [13]. During development, *Ascl1* controls

110   proliferation, cell cycle exit, and full neuronal differentiation and specification of neural

111   progenitor cells in both the central and peripheral nervous systems [11, 14, 15]. *Ascl1*

112   inhibits its own expression by negative autoregulation in the developing nervous

113   system, possibly explaining the lack of overt abnormalities in *Ascl1*^{+/-} mice [16], whereas

114   *Ascl1*^{-/-} pups die within hours after birth due to defects in brain development [10]. In the

115   adult, ASCL1 is expressed only in the brain and spinal cord where there is ongoing

116   neurogenesis, and in developing neuroendocrine cells in multiple organs including the

117   cerebellum, thyroid, and thymus [17]. In this study, we evaluated the activation, and

118   explored the function, of *Ascl1* in maternal livers of pregnant mice. We found that *Ascl1*

119   not only modulates maternal hepatic adaptation, but also mediates the communication

120   of maternal liver with other maternal organs and the placenta, eventually affecting

121   pregnancy outcomes.

122

123

Materials and methods

125

Mice

*Ascl1^fl/fl^;R26^EYFP/EYFP^* mice were a generous gift from Dr. Francois Guillemot (The Francis Crick Institute, Midland Road, London NW 1AT, UK) [18]. The mice are referred hereafter as *Ascl1^fl/fl^* for simplicity. C57BL/6 mice were purchased from the Jackson Laboratory (Bar Harbor, ME, USA). Mice were maintained on a 12-hour light/12-hour dark cycle (7 AM on and 7 PM off) at 22 ± 1°C and given a standard rodent chow and water *ad libitum*. All of the animal experiments were conducted in accordance with the National Institutes of Health *Guide for the Care and Use of Laboratory Animals*. The protocols for the care and use of animals were approved by the Indiana University-Purdue University Indianapolis Animal Care and Use Committee.

136

Mouse genotyping

Genomic DNA was prepared from mouse ear snips using the modified HotSHOT method [19]. All mice were genotyped by polymerase chain reaction (PCR) using KAPA Taq PCR Kits (Kapa Biosystems, Inc., Wilmington, MA, USA). Specific primers purchased from Integrated DNA Technologies (Coralville, IA, USA) were used to detect the wild type and mutant alleles (Supplemental Table 1). Primers *Ascl1* Forward and *Ascl1* WT Reverse were used to detect the *Ascl1* wild type allele (342 bp), and primers *Ascl1* Forward and *Ascl1* Mutant Reverse were used to detect floxed *Ascl1* allele (857 bp) [20]. PCR conditions were 35 cycles of 94°C/30 sec; 69°C/30 sec; 72°C/90 sec.

146

Timed pregnancy and virus injection

Timed pregnancy was generated by mating 3-month-old virgin $Ascl1^{fl/fl}$ female mice with wild type male mice to ensure heterozygous fetuses with one wild type $Ascl1$ allele. The presence of a copulation plug in the vagina was designated as gestation day (GD) 1. Adeno-associated virus serotype 8 (AAV8) with the thyroxine-binding globulin promoter (TBG) promoter expressing Cre (Addgene, AV-8-PV1091) were injected via tail vein at a dose of 1×10^{12} genomic copies per mouse on GD8, and mice were sacrificed on GD15 and GD18 using cervical dislocation. Adeno-associated viruses with a null vector (Addgene, AV-8-PV0148) were used as controls.

Tissue collection and histology

Mice were euthanized at various time points. Maternal liver, pancreas, spleen, and kidney organs, and placentas and fetuses were collected and weighed. Part of each tissue was fixed in 10% neutral buffered formalin (NBF), embedded in paraffin and sectioned at 5 μm for hematoxylin and eosin (H&E) staining and histological analysis. Meanwhile, part of each tissue was embedded in optimal cutting temperature (OCT) compound (Fisher Scientific, 23-730-571) on heptane cooled in dry ice and stored at -80°C until processing. The remaining tissues were snap-frozen in liquid nitrogen and stored at -80°C for protein and RNA extraction.

Immunohistochemistry

168 Formalin-fixed and paraffin-embedded (FFPE) maternal liver sections were subjected to

169 standard immunohistochemistry. Primary antibodies against β-Catenin (BD

170 Transduction, 610153, 1:100), IGF2 (R&D Systems, AF792, 1:1,000), and Ki67 (Thermo

171 Fisher Scientific, RM-9106-S1, 1:100) were used for immunostaining. The slide images

172 were acquired by the Leica DM2000 microscope using the Leica Application Suite

173 program. β-Catenin-positive or Ki67-positive hepatocytes in five random fields of view at

174 X400 magnification were counted using ImageJ software[21]. Periodic Acid Schiff staining

175 was performed on FFPE placental sections in 0.5% periodic acid solution (Santa Cruz,

176 sc-215695) and counterstained in hematoxylin (Leica, 3801575).

177

178 **Western blotting**

179 Liver and placental homogenates (10-30 µg) were separated by polyacrylamide gel

180 electrophoresis under reducing conditions and transferred to polyvinylidene difluoride

181 (PVDF) membranes. The following antibodies were used: p-AKT (T308, abcam,

182 ab76297, 1:5,000), p-AKT (S473, Epitomics, 2118-1, 1:2,000), ASCL1 (R&D Systems,

183 BAF2567, 1:500), ERK1/2 (Cell Signaling, 9102, 1:2,000), p-ERK1/2 (T202/Y204, Cell

184 Signaling, 4377, 1:2,000), GAPDH (Cell Signaling, 5174, 1:2,000), IGF2 (ABclonal,

185 A2086, 1:1,000), Lamin B1 (Cell Signaling, 9087, 1:1,000), and PL-II (gift from Dr.

186 Soares at the University of Kansas Medical Center, 1:2,000). Immune complexes were

187 detected by SuperSignal West Pico PLUS Chemiluminescent Substrate (Thermo Fisher

188 Scientific, 34577). Signals were detected using ImageQuant LAS 4000 Mini (General

189 Electric Life Sciences) and quantified using ImageJ software [21].

190

In situ hybridization

In situ hybridization was performed using RNAscope 2.5 HD Assay (Advanced Cell Diagnostics, 322310 and 322360) and appropriate probes and as per directions by the manufacturer. The following probes were used: *Ascl1* (Advanced Cell Diagnostics, 476321), *Igf2* (Advanced Cell Diagnostics, 437671), *PL-I* (Advanced Cell Diagnostics, 405521), and *PL-II* (Advanced Cell Diagnostics, 423681). A positive control probe *Ppib* (Advanced Cell Diagnostics, 310043) and a negative control probe *DapB* (Advanced Cell Diagnostics, 313911) were used to determine the efficacy of the protocol. These probes were applied to formalin-fixed and paraffin-embedded sections of mouse livers and placentas. The slide images were acquired by the Leica DM2000 microscope using the Leica Application Suite program. After approval from the institutional review boards, the laboratory information systems of our institute were searched. A set of paraffin blocks archived in the Department of Pathology of Indiana University School of Medicine were selected. They represented liver tissues from pregnant patients and patients with hepatocellular carcinoma or hepatocellular adenoma. These paraffin blocks were sectioned for *in situ* hybridization with a human Ascl1 probe (Advanced Cell Diagnostics, 459721).

Quantitative real-time polymerase chain reaction (qRT-PCR)

Total RNA was isolated from snap-frozen liver tissue using TRIzol reagent (Invitrogen, 15596018) as per directions by the manufacturer. Complementary DNA (cDNA) was synthesized from 1 μg of total RNA using Verso cDNA kit (Thermo Fisher Scientific, AB1453B) and diluted four times with water. Quantitative real-time polymerase chain reaction (qRT-PCR) was performed using the diluted cDNA with either TaqMan Gene Expression Master Mix (Applied Biosystems, 4369016) or PowerUp SYBR Green Master Mix (Applied Biosystems, A25742) with specific gene probes **(Supplemental Tables 2 and 3)** [22]. qRT-PCR was performed using the 7300 Real-Time PCR System

216   (Applied Biosystems) and analyzed by the 7300 System SDS RQ Study Software

217   (Applied Biosystems). qRT-PCR conditions for probes **(Supplemental Tables 2)** using

218   TaqMan Gene Expression Master Mix were uracil N-glycosylase (UNG) incubation

219   (50°C/2 min), polymerase activation (95°C/10 min), and 40 cycles of PCR (95°C/15 sec,

220   60°C/1 min). qRT-PCR conditions for probes **(Supplemental Tables 3)** using PowerUp

221   SYBR Green Master Mix were uracil-DNA glycosylase (UDG) activation (50°C/2 min),

222   polymerase activation (95°C/2 min), 40 cycles of PCR (95°C/15 sec, 60°C/15 sec,

223   72°C/1 min), and dissociation curve (95°C/15 sec, 60°C/30 sec, 95°C/15 sec). Relative

224   gene expression was calculated by the comparative C_T method (ΔΔCt) and normalized

225   to 18S rRNA transcript levels.

226

227   **RNA sequencing**

228   Total RNA was isolated from snap-frozen liver tissue using the RNeasy Plus Mini Kit

229   (Qiagen, 74134) as per directions by the manufacturer. RNA sequencing was performed

230   and analyzed by the Center for Medical Genomics Core (Indiana University School of

231   Medicine). In brief, total RNA concentration and quality were assessed using Agilent

232   2100 Bioanalyzer. Single-indexed strand-specific cDNA library from total RNA samples

233   (500 ng input with RIN ≥ 5) was prepared using TruSeq Stranded mRNA Library Prep

234   Kit (Illumina) as per directions by the manufacturer. The quality and size distribution of

235   the libraries were assessed using Qubit and Agilent 2100 Bioanalyzer. Libraries (200

236   pM) were clustered and amplified on cBot using HiSeq 3000/4000 PE Cluster Kit and

237   sequenced (2x75 bp paired-end reads) on HiSeq4000 (Illumina) using HiSeq 3000/4000

238   PE SBS Kit. A Phred quality score (Q score) was used to measure the quality of

239   sequencing. The quality of the sequencing data was assessed using FastQC

240   (Babraham Bioinformatics, Cambridge, UK). All sequenced libraries were mapped to the

241   mouse genome (UCSC mm10) using STAR RNA-seq aligner, reads distribution across

242   the genome was assessed using bamutils (from ngsutils), and uniquely mapped

243   sequencing reads were assigned to mm10 refGene genes using featureCounts (from

244   subread). Genes with CPM < 0.5 in more than 5 of the samples were removed. The

245   data were normalized using the TMM method. Differential expression analysis was

246   performed using edgeR and Ingenuity Pathway Analysis (IPA) with +/- 2-fold change

247   and $P < 0.05$. False discovery rate (FDR) was computed from p-values using the

248   Benjamini-Hochberg procedure.

249

250   **Serum biochemistry**

251   Blood from nonpregnant and pregnant mice (GD15 and GD18) was collected and left to

252   clot at room temperature. After two centrifugations at 3000 RPM, serum was collected

253   and analyzed by the Eli Lilly and Company (Indianapolis, IN). Serum insulin levels were

254   measured by the Translation Core at the IU School of Medicine Center for Diabetes and

255   Metabolic Diseases (Indiana University School of Medicine). Serum IGF2 levels were

256   quantified using a 1/6 dilution with the Mouse IGF-2 ELISA Kit (Boster Biological

257   Technology, EK0381) as per directions by the manufacturer and read with the

258   SpectraMax M2e spectrophotometer using the SoftMax Pro 6 program.

259

260   **Microbiome 16S sequencing**

261   Total microbial DNA was isolated from the snap-frozen cecal sample using the PureLink

262   Microbiome DNA Purification Kit (Invitrogen, A29789) as per directions of the

263   manufacturer. Microbiome 16S sequencing was performed and analyzed by the Zymo

264   Research Corporation (Irvine, CA). In brief, bacterial 16S ribosomal RNA gene targeted

265   sequencing was performed using the Quick-16S NGS Library Preparation Kit (Zymo

266   Research, Irvine, CA). The bacterial 16S primers, custom-designed by Zymo Research,

267   amplified the V3-V4 region of the 16S rRNA gene. The sequencing library was prepared

268   using PCR reactions in real-time PCR machines to control cycles and therefore prevent

269   PCR chimera formation. The final PCR products were quantified with qPCR

270   fluorescence readings and pooled together based on equal molarity. The final pooled

271   library was cleaned up with Select-a-Size DNA Clean & Concentrator (Zymo Research,

272   Irvine, CA), then quantified with TapeStation and Qubit. The final library was sequenced

273   on Illumina MiSeq with a v3 reagent kit (600 cycles). The sequencing was performed

274   with >10% PhiX spike-in. Amplicon sequences were inferred from raw reads using the

275   Dada2 pipeline. Chimeric sequences were also removed with the Dada2 pipeline.

276   Taxonomy assignment, composition bar charts, alpha-diversity, and beta-diversity

277   analyses were performed with Qiime v.1.9.1. Taxa that have an abundance significantly

278   different among groups were identified by LEfSe with default settings if applicable.

279   Differential expression analysis was assessed using IPA with +/- 2-fold change and $P <$

280   0.05.

281

282   **β-Cell mass**

283 Pancreatic tissues were fixed in 4% paraformaldehyde (PFA) (Sigma Aldrich, 818715),

284 embedded in paraffin, and sectioned at 7 μm for collecting 5 sections at 50 μm apart per

285 pancreatic sample. Pancreatic sections immunostained for Insulin (Santa Cruz, sc-

286 9168, 1:100) were used to quantify insulin-positive β-cell mass. β-Cell mass was

287 determined by the ratio of the insulin-positive stained area to the tissue area multiplied

288 by the pancreas weight.

289

290 **Statistical analysis**

291 Data are shown as means ± standard deviation (SD) or means ± standard error of the

292 mean (SEM). Statistical analyses were performed using a two-sided unpaired Student's

293 t-test with the means ± 95% confidence intervals. Significant differences were defined

294 when $P < 0.05$.

295

296 **Results**

297

298 ***Ascl1* is highly activated in maternal hepatocytes.**

299 We first evaluated the expression of *Ascl1* in maternal livers throughout the course of

300 gestation in mice. As pregnancy advanced, its transcript levels in maternal livers were

301 progressively elevated, reaching up to 26,000-fold on gestation days 13 and 15, relative

302 to the pre-pregnancy state (Fig. 1A). Maternal hepatic *Ascl1* protein was abundantly

303 expressed as its mRNA levels peaked on these two gestation days (Fig. 1B). *Ascl1*

304 transcript was detected exclusively in maternal hepatocytes (Fig. 1C). In humans, *Ascl1*

305 mRNA was abundantly expressed in a maternal liver of a pregnant woman, and in liver

306   diseases such as hepatocellular carcinoma, hepatocellular adenoma, and hepatitis (Fig.

307   1D). Thus, it is truly astonishing that pregnancy activates a proneuronal transcription

308   factor in an epithelial cell type in such a striking magnitude in a maternal compartment

309   of pregnant animals and humans, strongly suggesting a gestation-dependent role for

310   this transcription factor.
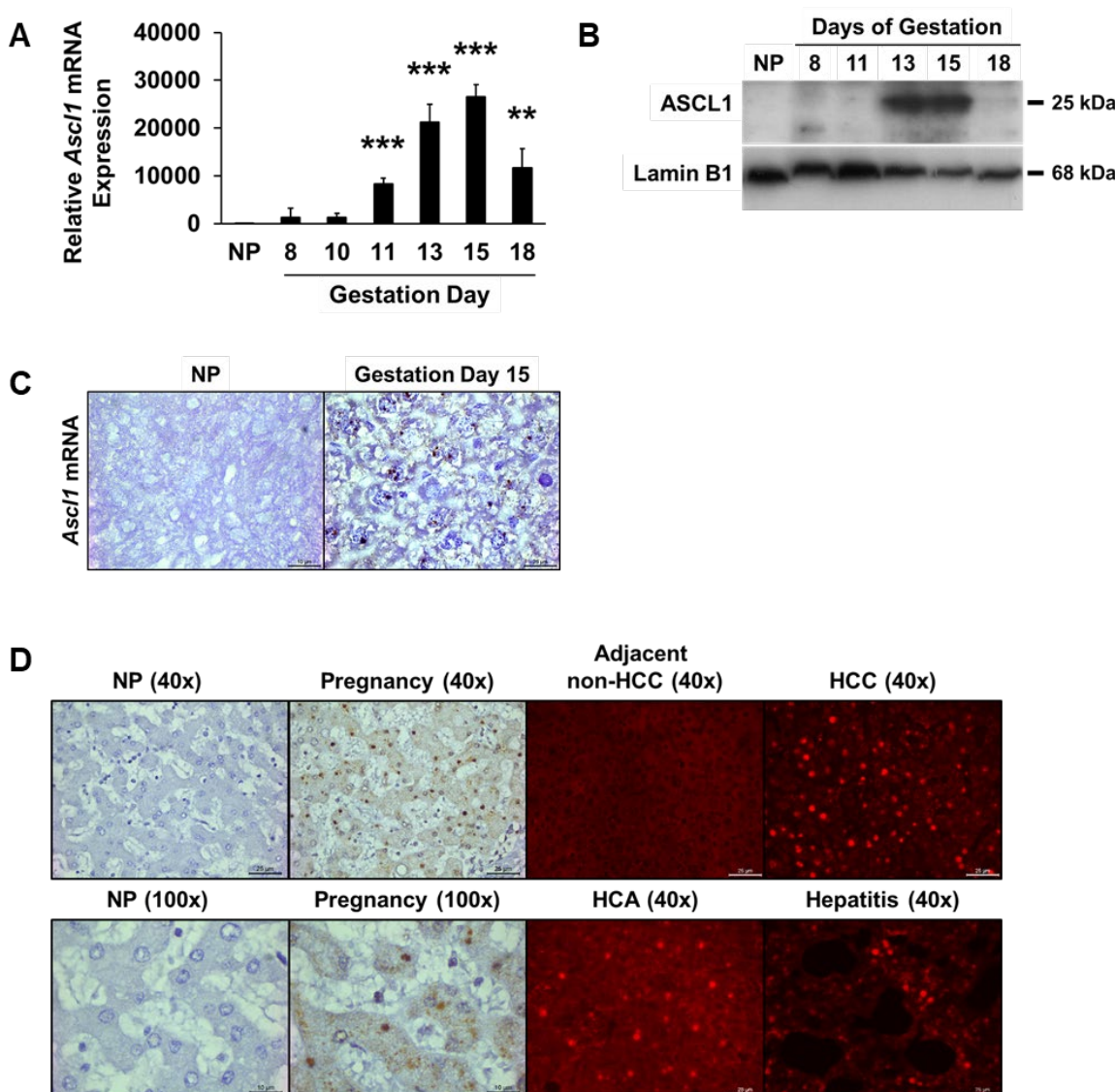
311

Lee_Fig1

312

Fig. 1. *Ascl1* activation and *Ascl1*-dependent transcriptome in maternal livers of pregnant mice.

Timed pregnancies were generated in 3-month-old C57BL/6 female mice. Livers were collected from non-pregnant (NP) mice and maternal livers from pregnant mice at the indicated gestation days (GD). **(A-C)** *Ascl1* expression in maternal livers. **(A)** Hepatic *Ascl1* mRNA levels were measured using qRT-PCR and presented as the mean fold changes relative to NP controls ± SD (n = 3). **, $P < 0.01$; ***, $P < 0.001$, compared with NP controls. **(B)** Western blotting was performed using liver nuclear lysates with antibodies against ASCL1. Lamin B1 was used as a loading control. **(C)** Liver sections were subjected to *Ascl1 in situ* hybridization. *Ascl1* mRNA is stained dark brown. **(D)** Liver sections were prepared from archived paraffin blocks of human liver tissues. *Ascl1* mRNA were visualized on liver sections. Representative results are shown with liver sections from a nonpregnant (NP) woman (a 6-month pregnant mother), a hepatocellular carcinoma (HCC) patient, a hepatocellular adenoma (HCA) patient, and a 4.5-month child with hepatitis.

Adeno-associated virus 8 (AAV8) containing the gene for *Cre* recombinase under the control of hepatocyte-specific thyroxine-binding globulin (*TBG*) promoter (AAV8-TBG-Cre) efficiently deletes *Ascl1* in maternal hepatocytes.

Ascl1 is activated in maternal liver during the second half of pregnancy, suggesting a role in the maintenance of pregnancy. To determine this, we took a loss-of-function approach to delete the *Ascl1* gene specifically in maternal hepatocytes from mid-gestation to term and evaluated how pregnancy was affected. We generated timed pregnancies in *Ascl1*$^{fl/fl}$ female mice by mating them with *Ascl1*$^{+/+}$ males. This led to a homogeneous *Ascl1*$^{+/fl}$ fetal genotype. AAV8-TBG-Cre virus or AAV8-TBG-null (control) virus was injected into *Ascl1*$^{fl/fl}$ mice on gestation day 8. Mice were sacrificed on gestation days 15 and 18 for phenotypic assessment. This AAV8-TBG virus has been shown to specifically infect hepatocytes with >99% efficiency in mice [23, 24]. qRT-PCR

338   analysis showed that *Ascl1* mRNA was almost completely lost in maternal livers of

339   pregnant animals treated with the AAV8-TBG-Cre virus (Fig. 2A), indicating highly

340   efficient *Ascl1* gene deletion in this organ. As such, mice deficient for *Ascl1* in maternal

341   hepatocytes were referred to as hep-*Ascl1*$^{-/-}$ mice hereafter. Of note, in a pretest study,

342   we injected AAV8-TBG-GFP reporter virus into pregnant mice. As a result, we detected

343   GFP expression in maternal livers but not in fetal livers (data not shown). This indicates

344   that the AAV8 virus does not effectively pass through the placenta to infect the fetuses.

345

346   **RNA-sequencing (RNA-seq) analysis reveals *Ascl1*-dependent transcriptome in**

347   **maternal liver.**

348   We next compared the transcriptomes of gestation day 15 maternal livers between the

349   two genotype groups of mice by RNA-seq to profile potential Ascl1 target genes in this

350   context. This revealed 1,274 differentially expressed genes. They were either up-

351   regulated or down-regulated by at least 2-fold with a false discovery rate of less than

352   0.05 when maternal hepatic *Ascl1* was lacking (Fig. 2B). Pathway analysis suggests

353   that these genes are associated with many biological processes including the

354   metabolism of hormones (e.g. melatonin), neurotransmitters (e.g. serotonin and

355   dopamine), fatty acids, alcohol, carbohydrates, nucleic acids, and amino acids, cell

356   cycle control, cell function and maintenance, and vitamin D receptor/retinoid X receptor

357   activation (Fig. 2C). These data imply that *Ascl1* directly or indirectly regulates a broad

358   spectrum of genes and thereby possesses multiple functions in maternal liver in this
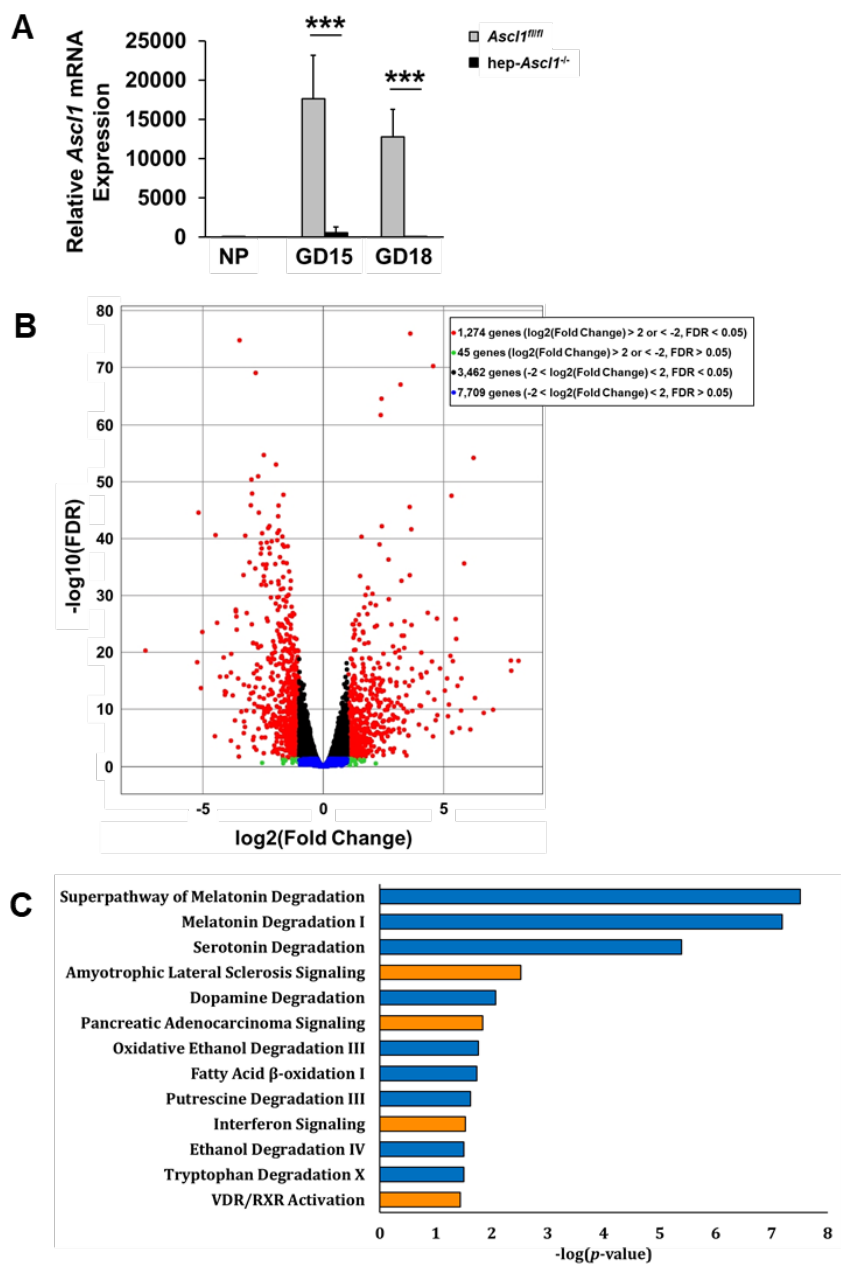
359   physiological state (pregnancy).

360

Fig. 2. Differentially expressed genes and canonical pathways affected by hepatocyte-specific deletion of *Ascl1* in the maternal liver. (A) Total RNA was isolated from livers of nonpregnant (NP) and pregnant *Ascl1fl/fl* and hepatocyte-specific Ascl1 knockout (hep-*Ascl1-/-*) mice. Hepatic *Ascl1* mRNA levels were measured using qRT-PCR and presented as the mean fold changes relative to NP controls ± SD (n = 4-5). ***, $P < 0.001$. **(B-C)** *Ascl1*-dependent transcriptome. Total RNA was isolated from livers of

367   *Ascl1^{fl/fl}* and hep-*Ascl1^{-/-}* mice on gestation day (GD) 15 and was subjected to RNA-sequencing (n = 4-5).

368   **(B)** Differentially expressed genes are presented by the volcano plot. Red: significantly up- or down-

369   regulated genes; black, green, and blue: non-significant genes. Differentially expressed genes with at

370   least two-fold and *P* < 0.05 were analyzed using the Ingenuity Pathway Analysis (IPA). **(C)** Top enriched

371   canonical pathways targeted by hepatic *Ascl1* are presented. Orange, up-regulated; blue, down-

372   regulated.

373

374   **Hepatocyte-specific *Ascl1* knockout results in maternal liver abnormalities.**

375   We subsequently assessed whether maternal livers exhibited *Ascl1*-dependent

376   phenotypes. Compared with maternal hepatocytes sufficient for *Ascl1*, maternal

377   hepatocytes lacking *Ascl1* displayed an aberrant structure (eosin staining-negative

378   around the nuclei) (Fig. 3A), enhanced hepatocyte proliferation (Fig. 3B, Supplemental

379   Fig. 1A), and increased size (Fig. 3C, Supplemental Fig. 1B), hence causing further

380   enlargement of the maternal livers (Fig. 3D-E). These abnormalities were accompanied

381   by reduced albumin mRNA expression and protein production and elevated circulating

382   alanine transaminase (ALT) and aspartate aminotransferase (AST) (Fig. 3F). These

383   observations indicate that *Ascl1* loss of function in maternal hepatocytes impairs their

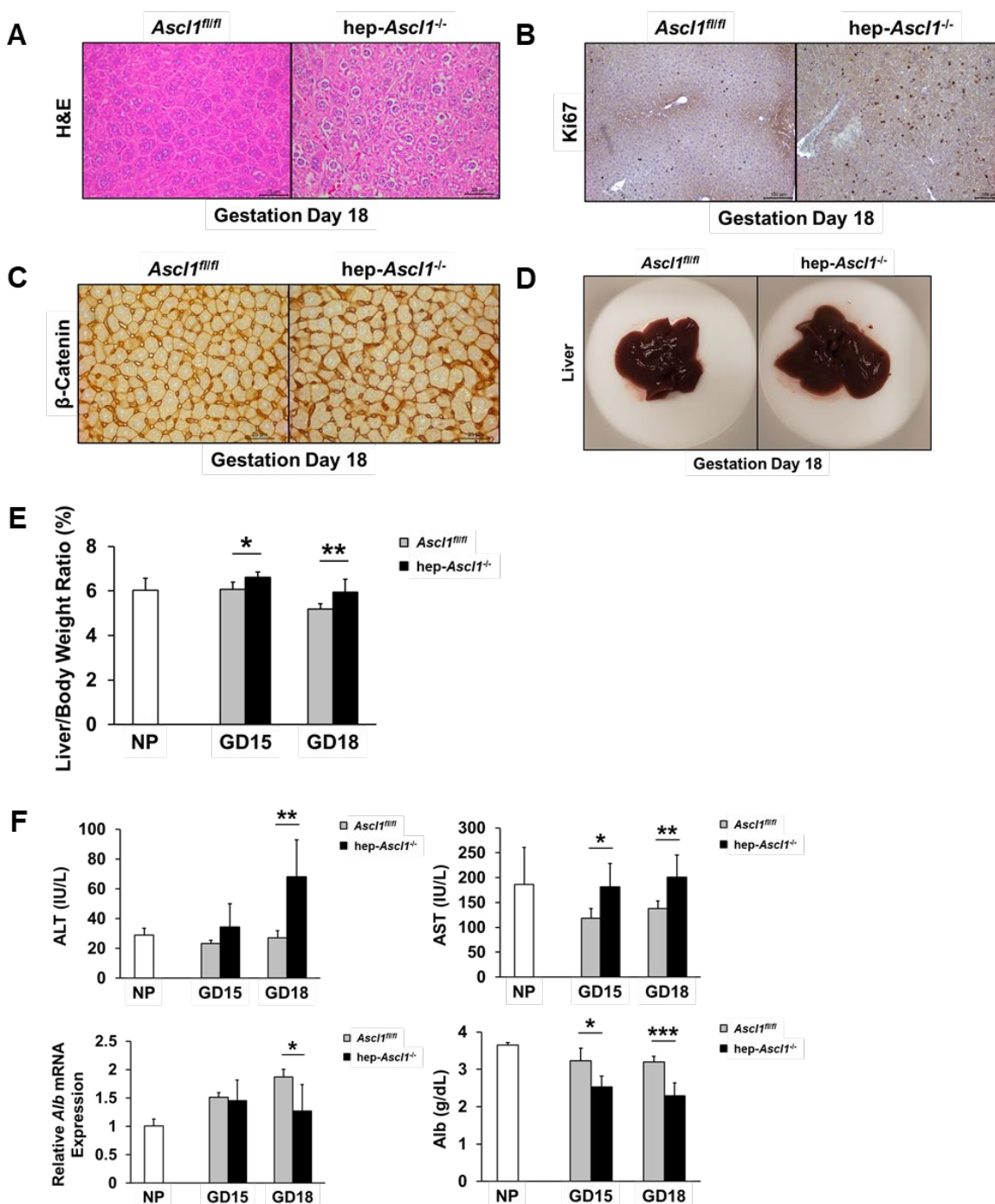384   structure and function.

385

386

Fig. 3. Maternal liver phenotypes in maternal hepatocyte-specific *Ascl1* ablated mice. Livers were

collected and weighed from nonpregnant (NP) and gestation days (GD) 15 and 18 *Ascl1*$^{fl/fl}$ and hep-*Ascl1*$^{-}$

$^{/-}$ mice. **(A)** Liver sections were stained with hematoxylin and eosin (H&E). Liver sections were subjected

390   to **(B)** Ki67 and **(C)** β-Catenin staining. **(D)** Morphology of *Ascl1*$^{fl/fl}$ and hep-*Ascl1*$^{-/-}$ mouse livers. **(E)** Liver-

391   to-body weight ratios are presented as means ± SD (n = 4-10). **(F)** Serums were collected from NP and

392   pregnant *Ascl1*$^{fl/fl}$ and hep-*Ascl1*$^{-/-}$ mice. Data of serum biochemical profile are expressed as means ± SD

393   (n = 5). Hepatic *Albumin* mRNA levels were measured using qRT-PCR and presented as the mean fold

394   changes relative to NP controls ± SD (n = 4-5). *, $P < 0.05$; **, $P < 0.01$; ***, $P < 0.001$.

395

396   **Hepatocyte-specific *Ascl1* knockout causes overgrowth of maternal pancreas,**

397   **spleen, and kidney.**

398   We additionally examined several other maternal organs to estimate whether there were

399   *Ascl1*-dependent systemic effects in the maternal compartment. Surprisingly, without

400   maternal hepatic *Ascl1*, the maternal pancreas nearly doubled in size (Fig. 4A-B), had a

401   reduced proportion of insulin-positive areas (Fig. 4C-D), and unchanged total β-cell

402   mass (Fig. 4E), while the concentrations of circulating insulin and non-fasting blood

403   glucose were unaltered (Supplemental Fig. 2). These data suggest that *Ascl1*

404   inactivation in maternal liver stimulates the expansion of the exocrine component

405   without interfering with the pregnancy-dependent growth of the endocrine component in

406   the maternal pancreas. Similarly, the maternal spleen also almost doubled in volume

407   with overtly expanded red and while pulps (Fig. 5A-C), while the maternal kidney

408   showed enlargement without an obvious histological alteration (Fig. 5D-E). Collectively,

409   we conclude that the loss of function of *Ascl1* in maternal hepatocytes imposes

410   systematic effects, causing overgrowth of at least a subset of maternal organs.
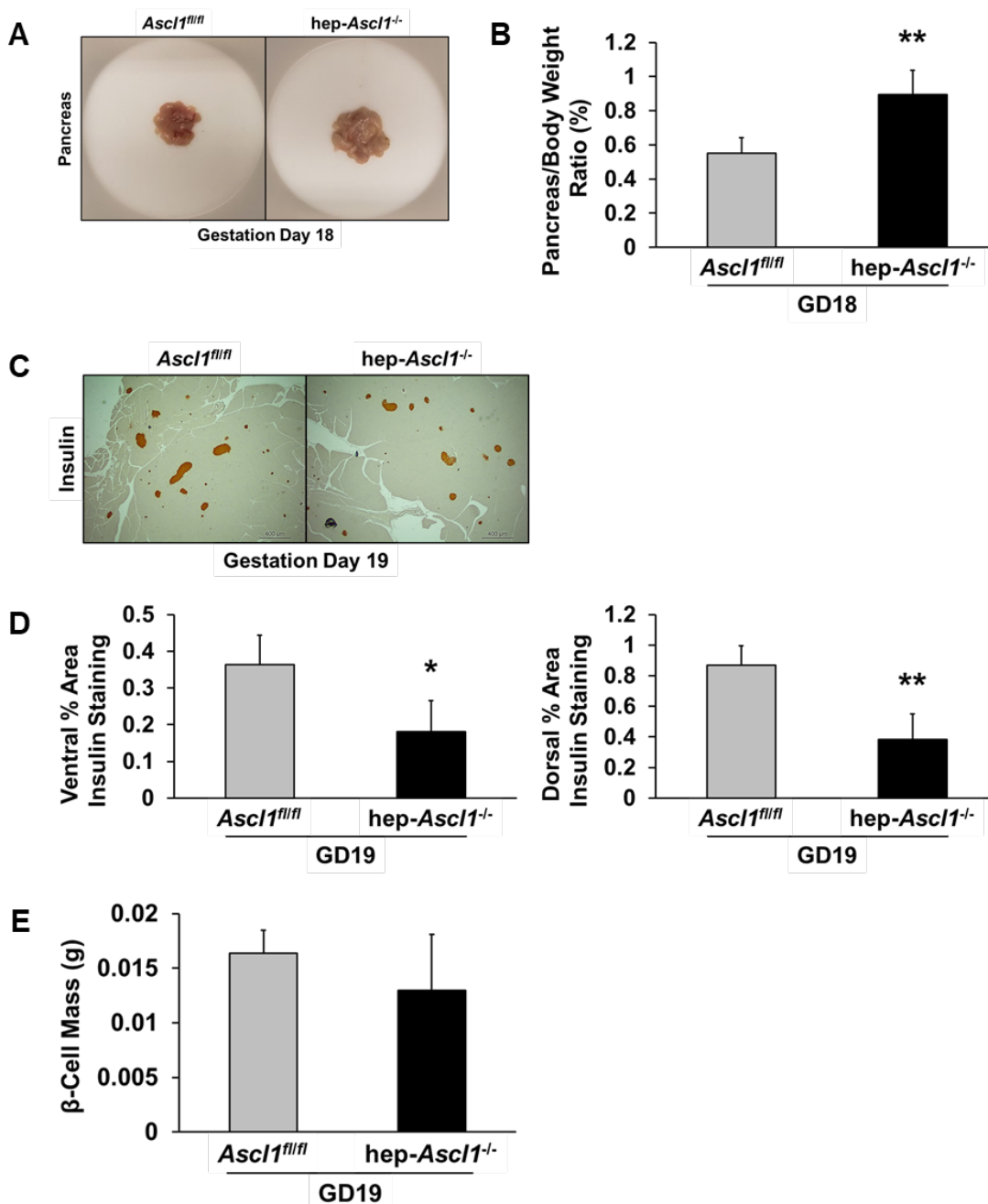
411

Fig. 4. Maternal pancreas phenotypes in maternal hepatocyte-specific *Ascl1* ablated mice. Maternal pancreases were collected and weighed from nonpregnant (NP) and gestation day (GD) 18 *Ascl1^{fl/fl}* and hep-*Ascl1^{-/-}* mice. **(A)** Morphology of the pancreas. **(B)** Pancreas-to-total body weight ratios are presented as means ± SD (n = 4-5). **(C)** Pancreatic sections were subjected to insulin immunostaining. **(D)** The

417 quantification of the insulin-positive islets to the pancreatic section area are presented as means ± SD (n

418 = 4-5). **(E)** β-Cell mass is presented as the means ± SD (n = 4-5). *, $P < 0.05$; **, $P < 0.01$.
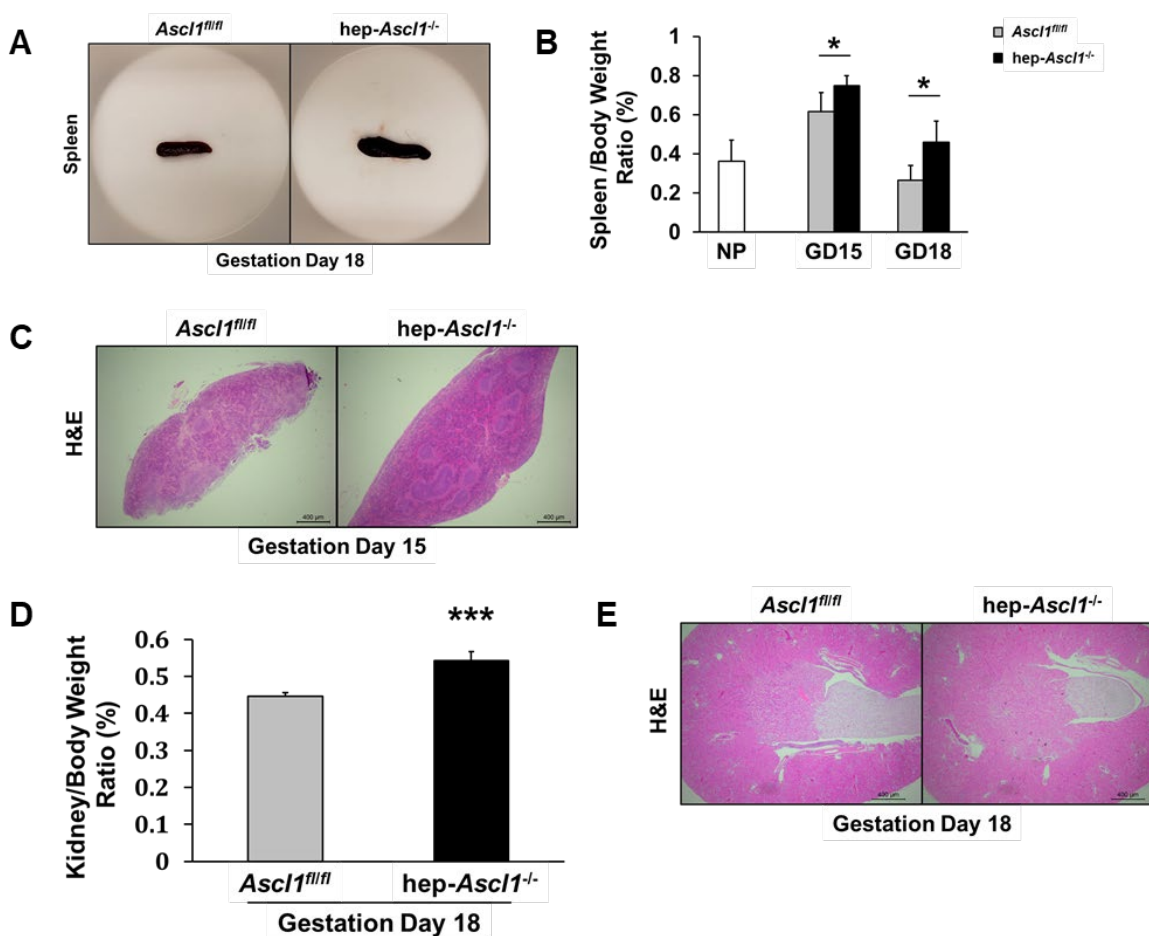
419

Lee_Fig5

420

421 **Fig. 5. Maternal spleen and kidney phenotypes in maternal hepatocyte-specific *Ascl1* ablated**

422 **mice.** Maternal spleens and kidneys were collected and weighed from nonpregnant (NP) and gestation

423 days (GD) 15 and 18 *Ascl1*$^{fl/fl}$ and hep-*Ascl1*$^{-/-}$ mice. **(A)** Morphology of the spleens. **(B)** Spleen-to-total

424 body weight ratios are presented as means ± SD (n = 4-10). **(C)** Splenic sections were stained with

425 hematoxylin and eosin (H&E). **(D)** Kidney-to-total body weight ratios are presented as means ± SD (n = 4-

426 5). **(E)** Kidney sections were stained with H&E. *, $P < 0.05$; ***, $P < 0.001$.

427

428 **Hepatocyte-specific *Ascl1* knockout leads to abnormal maternal cecal microbiota.**

429 It is known that the maternal gut microbiome undergoes pregnancy-dependent changes,

430 which are associated with the health of both the mother and the fetus [25]. To determine

431 whether maternal hepatic *Ascl1* is relevant to the maternal microbiome, we collected

432 maternal cecal contents from gestation day 18 hep-*Ascl1*^{-/-} mice and *Ascl1*^{fl/fl} (control)

433 mice, and compared their microbiome profiles via 16S sequencing (Fig. 6A). Most

434 notably, *Ascl1* loss in maternal hepatocytes resulted 1) in a complete depletion of

435 *Pseudobutyrivibrio-Roseburia intestinalis*, which protects colonic mucosa against

436 inflammation [26], 2) in the appearance of *Desulfovibrio oxamicus-vulgaris*, which

437 metabolizes a variety of chemicals [27], and 3) in alterations in the relative abundance of 6

438 other bacteria species. Furthermore, RNA-seq analysis revealed that *Hamp2*, a gene

439 encoding hepcidin antimicrobial peptide 2, which has a strong antimicrobial activity

440 against certain bacteria [28, 29], depends on Ascl1 for expression. This finding was

441 confirmed by qRT-PCR (Fig. 6B). Together, we demonstrate that maternal hepatic

442 *Ascl1* modulates the adaptation of the maternal microbiota to pregnancy, potentially via
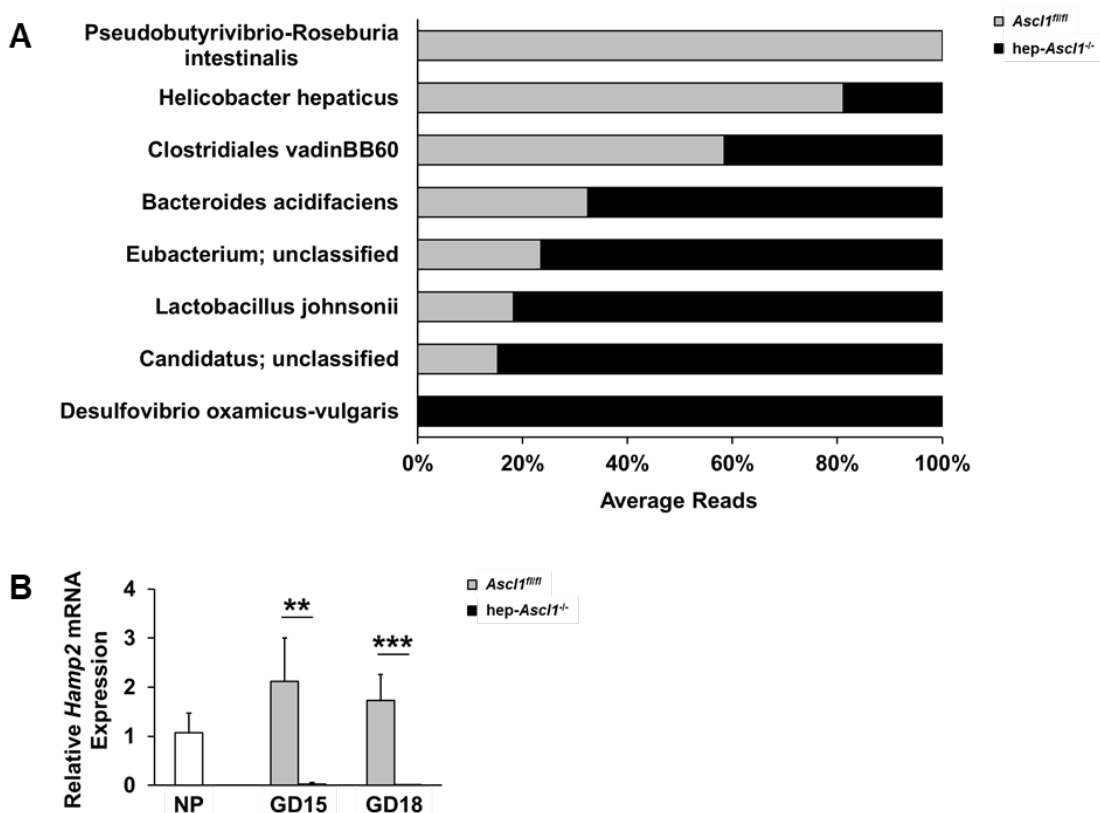
443 regulating *Hamp2*.

444

Fig. 6. Phenotypes of maternal cecal microbiota in maternal hepatocyte-specific *Ascl1* ablated

mice. Maternal cecal samples were collected from gestation day (GD) 18 *Ascl1^fl/fl^* and hep-*Ascl1^-/-^* mice.

(A) Cecal microbiota analysis (n = 5). **(B)** Hepatic hepcidin antimicrobial peptide 2 (*Hamp2*) mRNA levels

were measured using qRT-PCR and presented as the mean fold changes relative to nonpregnant (NP)

controls ± SD (n = 4-5). **, $P < 0.01$; ***, $P < 0.001$.

Hepatocyte-specific *Ascl1* knockout causes placental overgrowth and aberrant

postnatal growth of offspring.

We examined the uteroplacental and fetal compartments and postnatal growth of pups

to determine whether *Ascl1* deficiency in maternal hepatocytes ultimately affects

456   pregnancy outcomes. Compared to the placentas of control mice, the placentas of hep-

457   *Ascl1*^{-/-} mice were markedly enlarged, manifested by a 26.9% increase in weight on

458   gestation day 15 and 33% on gestation day 18, with the expansion of both the junctional

459   and labyrinth zone (Fig. 7A-B). The distribution of glycogen trophoblast cells visualized

460   by glycogen staining did not appear to be *Ascl1*-dependent (Supplemental Fig. 3A). By

461   *in situ* hybridization, we probed the mRNAs of *placental lactogen (PL)-I*, a marker gene

462   for parietal trophoblast giant cells [30], and *PL-II*, a marker gene for parietal trophoblast

463   giant cells, spongiotrophoblast cells, and labyrinth trophoblast giant cells [30], and did not

464   observe an overt *Ascl1*-dependent distribution of these trophoblast cell populations

465   (Supplemental Fig. 3B). These results of placental structural evaluations suggest that

466   the loss of function of *Ascl1* in maternal hepatocytes causes placental overgrowth

467   without disrupting placental structure. Moreover, when comparing hep-*Ascl1*^{-/-} pregnant

468   mice with their control mice, the placental levels of insulin-like growth factor (IGF2), a

469   potent placental and fetal growth factor [31-33], were reduced by 32% on gestation day 15

470   but were equivalent on gestation day 18, whereas placental concentration of PL-II, a

471   major hormone produced by the placenta during the second half of gestation [34], was

472   unchanged (Fig. 7C, Supplemental Fig. 3C). However, when maternal hepatic *Ascl1*

473   was deficient, maternal blood concentration of alkaline phosphatase, an enzyme

474   primarily elaborated from the placenta and a marker for trophoblast differentiation [35],

475   was significantly elevated on gestation day 15 and more than 2-fold on gestation day

476   18. The data of these functional assessments suggest that *Ascl1* inactivation in

477   maternal hepatocytes partially influences placental function.

478   Furthermore, it is known that AKT and ERK signaling critically regulates placental

479   development and growth [36, 37]. We found that, without *Ascl1* in maternal hepatocytes,

480   placental AKT1 phosphorylation at S473, but not at T308, was mildly increased; in

481   contrast, ERK1 and ERK2 activities were dramatically inhibited, reduced as much as

482   80% and 76% respectively, prior to parturition (gestation day 18). Thus, the loss of

483   maternal hepatic *Ascl1* results in strong inhibition of placental ERK signaling.

484   Additionally, we did not observe a difference in fetal weight and number on both

485   gestation days 15 and 18 between the two genotype groups of mice (Supplemental Fig.

486   4). However, compared to those male and female pups born from control dams, male

487   pups born from hep-*Ascl1*$^{-/-}$ dams displayed a 16% increase in weekly body weight gain

488   at week 1 post-weaning, but a 41% decrease at week 2, while females pups born from

489   hep-*Ascl1*$^{-/-}$ dams exhibited a 32% increase at week 1, a 35% decrease at week 2, a

490   38% decrease at week 3, and a 43% increase at week 5 (Fig. 7D). Apparently, pups

491   born from the two genotype groups of dams grew quite differently after weaning. Taken

492   together, we demonstrate that the maternal hepatic *Ascl1* null mutation causes

493   placental overgrowth, partial changes in placental function, severe suppression of

494   placental ERK activity, and an abnormal postnatal growth pattern of offspring.
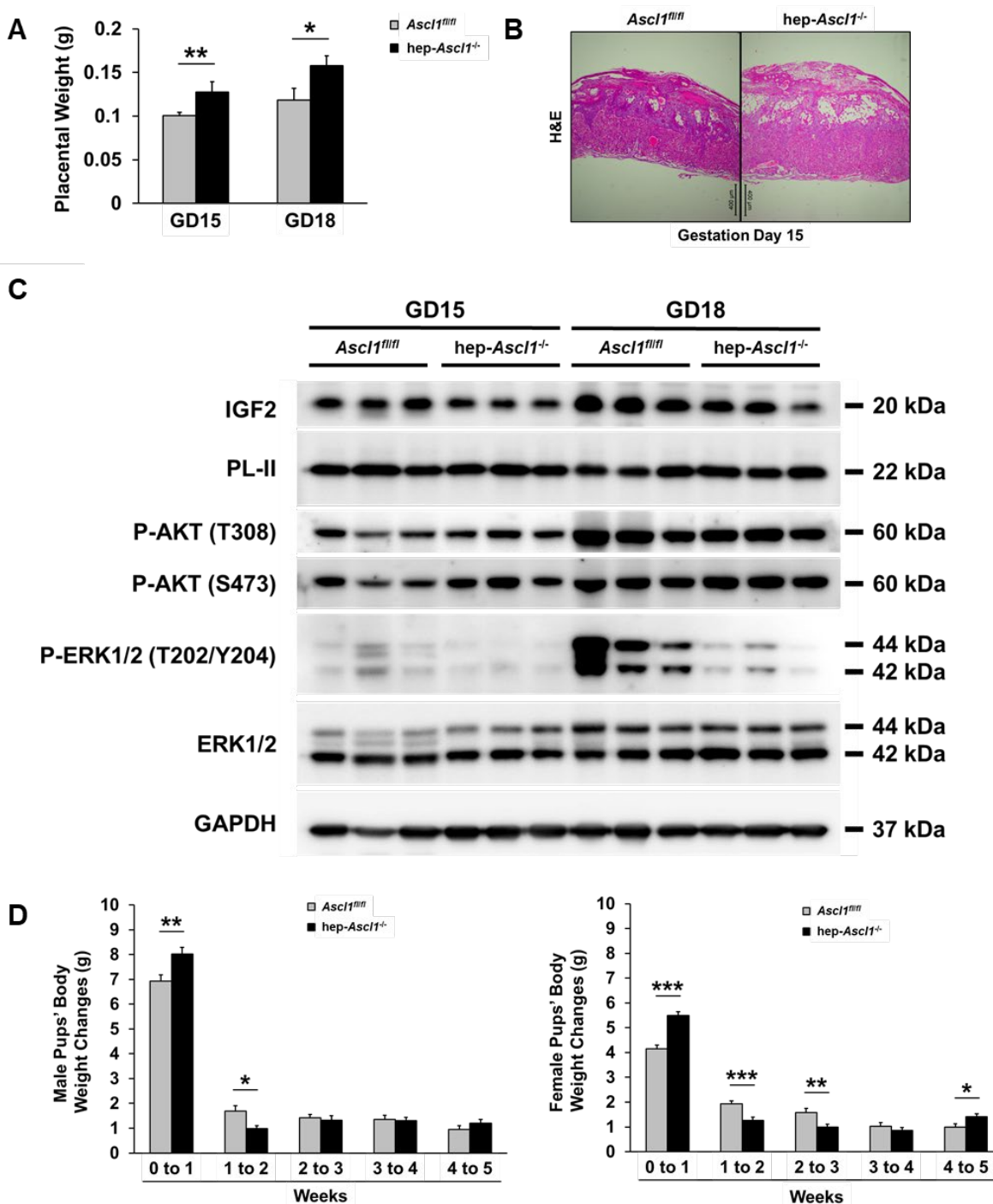
495

Fig. 7. Placental phenotypes in maternal hepatocyte-specific *Ascl1* ablated mice. Placentas were collected and weighed from gestation days (GD) 15 and 18 *Ascl1*^{fl/fl} and hep-*Ascl1*^{-/-} mice. **(A)** Placental weights are presented as means ± SD (n = 4-9 dams). **(B)** Placental sections were stained with

500   hematoxylin and eosin (H&E). **(C)** Western blotting was performed using placental lysates prepared from

501   one placenta per dam with antibodies against the proteins indicated. Glyceraldehyde 3-phosphate

502   dehydrogenase (GAPDH) was used as a loading control. **(D)** Weekly body weight changes of weaned

503   pups (n = 43 from 5 *Ascl1^fl/fl^* dams; n = 44 from 6 hep-*Ascl1^-/-^* dams; n = 6-10 per litter) are presented as

504   means ± SEM. *, *P* < 0.05; **, *P* < 0.01; ***, *P* < 0.001.

505

506   **Hepatocyte-specific *Ascl1* knockout leads to *Igf2* activation in maternal**

507   **hepatocytes.**

508   The above observations that several maternal organs were significantly enlarged in

509   hep-*Ascl1^-/-^* pregnant mice relative to controls prompted us to look for growth factors

510   regulated by *Ascl1* from our RNA-seq analysis. We found one candidate: *Igf2*, which

511   encodes a potent growth factor [31-33] and was induced with Ascl1 loss. To validate the

512   RNA-seq data, we quantified *Igf2* mRNA levels by qRT-PCR in maternal livers of

513   gestation days 15 and 18 and show that the loss of *Ascl1* in maternal hepatocytes

514   induced robust *Igf2* mRNA expression in maternal livers, most strikingly on gestation

515   day 18 (Fig. 8A). Consistently, maternal hepatic IGF2 protein was abundantly produced

516   in hep-*Ascl1^-/-^* pregnant mice, but was undetectable in control pregnant mice (Fig. 8B).

517   *In situ* hybridization and immunohistochemistry detected rich *Igf2* transcripts (Fig. 8C)

518   and IGF2 protein (Fig. 8D) in maternal hepatocytes deficient for *Ascl1*, but not in

519   controls (Fig. 8D). In mice, *Igf2* is maternally imprinted and is differentially regulated in

520   the placenta and fetus. It is transcribed from four promoters, designated *Igf2-P0, P1,*

521   *P2, and P3*. *Igf2-P0* directs *Igf2* transcription in the placenta, whereas *Igf2-P1, P2, and*

522   *P3* direct its transcription in both the placenta and fetus [32, 38]. We used a set of qRT-

523   PCR primers to analyze promoter-specific *Igf2* transcripts in maternal livers [39] (Fig. 8E).

524   We found that *P0* remained silent no matter the presence or absence of *Ascl1* in

525   maternal hepatocytes. In contrast, the other three promoters were all activated due to

526   *Ascl1* loss in these cells. The concentration of circulating IGF2 protein in gestation day

527   18 hep-*Ascl1*$^{-/-}$ mice was about 9 times higher than that in control mice (Fig. 8F). These

528   data collectively demonstrate that, in maternal hepatocytes, *Ascl1* deficiency results in

529   *Igf2* activation via *P1*, *P2*, and *P3*, creating a maternal environment rich in this growth

530   factor. Thus, here we linked *Igf2* to *Ascl1*-dependent phenotypes in our experimental

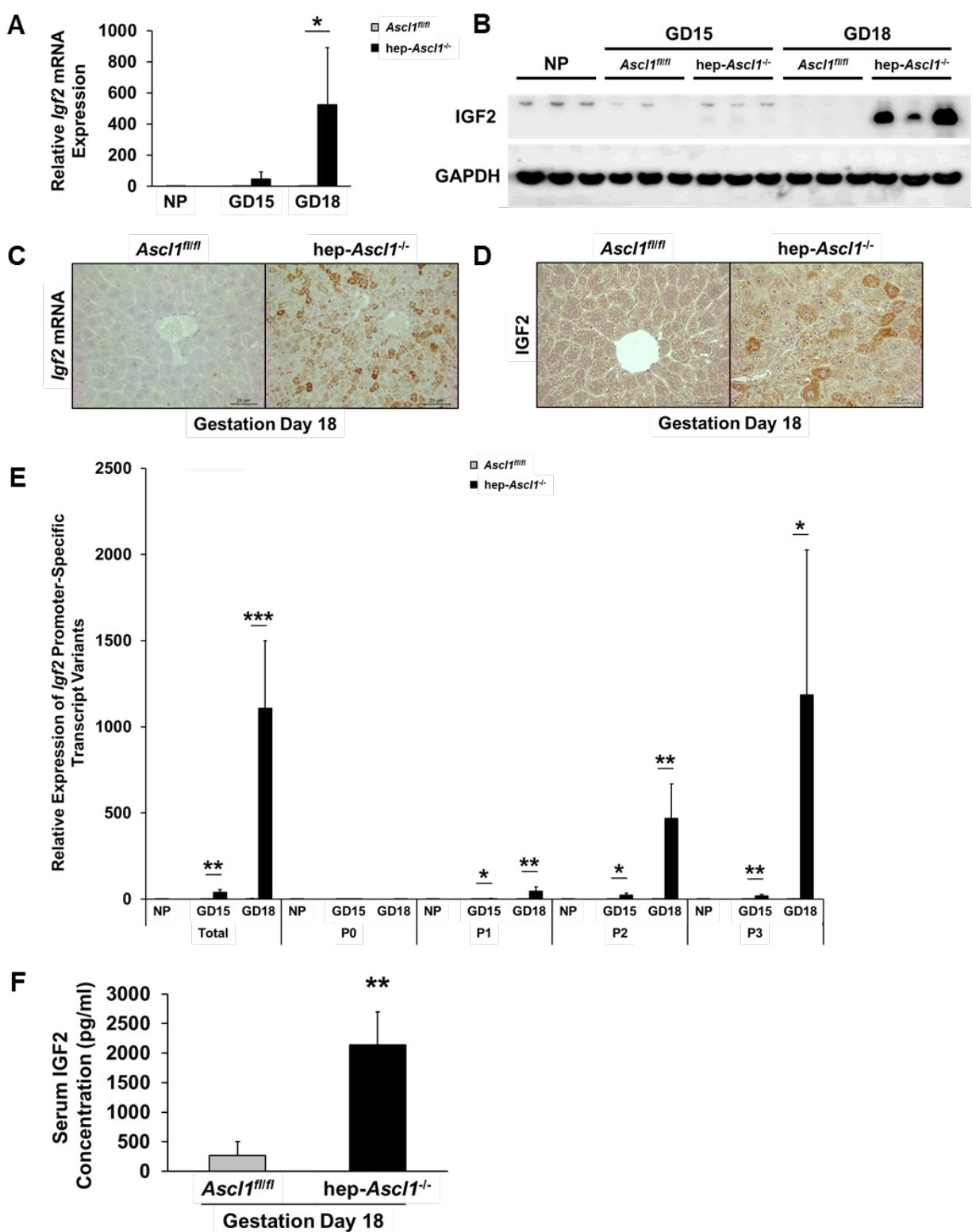531   settings.

532

Lee_Fig8

533

534 **Fig. 8. *Igf2* activation in maternal livers deficient for *Ascl1*.** Maternal livers were collected and

535 weighed from nonpregnant (NP) and gestation days (GD) 15 and 18 *Ascl1^fl/fl^* and hep-*Ascl1^-/-^* mice. **(A)**

536 Hepatic *Igf2* mRNA levels were measured using qRT-PCR and presented as the mean fold changes

537 relative to NP controls ± SD (n = 4-5). **(B)** Western blotting was performed using liver lysates with an

538 antibody against IGF2. **(C)** *Igf2 in situ* hybridization on liver sections. **(D)** IGF2 immunostaining. **(E)** Levels

539 of hepatic *Igf2* promoter-specific transcript variants were measured using qRT-PCR and presented as the

540 mean fold changes relative to NP controls ± SD (n = 4-5). **(F)** Levels of IGF2 protein in serum were

541 measured using ELISA and presented as the mean fold changes ± SD (n = 3-5). *, $P < 0.05$; **, $P < 0.01$;

542 ***, $P < 0.001$. P0, placental-specific *Igf2* promoter; P1-3, placental- and fetal liver-specific *Igf2* promoter.

543

Discussion

545

546 It has been an enigma why maternal liver activates a proneuronal gene (*Ascl1*) in

547 response to pregnancy. Here we demonstrate that *Ascl1* is required for the maternal

548 liver to structurally and functionally adapt to this physiological stimulus (pregnancy).

549 Loss of *Ascl1* in maternal hepatocytes impairs their cellular structure, reflected by the

550 formation of a layer of eosin staining-negative substance around their nuclei. This

551 substance was Oil Red O staining- and Periodic acid Schiff staining-negative,

552 suggesting that it is not a fatty acid or glycogen (data not shown). Others reported a

553 similar phenomenon in *Mst1/2* double knockout hepatocytes [40]. The connection

554 between Ascl1 and Mst1/2 signaling in maternal hepatocytes will be interesting to

555 explore in future. Although the eosin staining-negative substance around the hepatocyte

556 nuclei remains unknown, we believe that it is linked to *Ascl1* deficiency-caused

557 dysfunction of maternal hepatocytes, characterized by reduced albumin production and

558 increased ALT and AST release. In addition, *Ascl1* loss induced increased proliferation

559   and hypertrophy of maternal hepatocytes, which was associated with increased IGF2

560   production by these cells. IGF2 is a prototypical growth factor driving cell expansion and

561   organogenesis during development [41], and adult regenerating livers activate IGF2 to

562   promote hepatocyte replication [42]. Here we show that pregnancy reprograms maternal

563   hepatocytes to activate *Ascl1*, thereby controlling the transcriptional output and

564   modulating the expression of at least 1,274 genes. Of special note, the top canonical

565   pathway describing these differentially expressed genes is one that represents genes

566   involved in the metabolism of neurotransmitters. *Ascl1* is known to be essential for the

567   development of serotonergic and dopaminergic neurons and also regulates their

568   neurotransmitter biosynthesis [43, 44]. Remarkably, *Ascl1* alone is sufficient to generate

569   functional neurons from fibroblasts and embryonic stem cells, being a key driver of

570   induced neuronal cell reprogramming in different cell contexts [45]. These findings raise

571   the question of whether *Ascl1* activation enables maternal hepatocytes to possess

572   some properties of neurons as an adaptive response to support a healthy pregnancy.

573   We are very interested in answering this question in our future studies.

574

575   It is surprising that inactivating *Ascl1* in maternal liver induced robust systemic

576   responses in the maternal compartment. This implies that the maternal liver, via

577   activating *Ascl1*, communicates with other maternal organs to systematically coordinate

578   maternal adaptations to pregnancy, uncovering a novel function of maternal liver during

579   pregnancy. Moreover, we revealed an *Ascl1/Igf2* axis in maternal hepatocytes, where

580   Ascl1 normally silences the *Igf2* locus and thereby avoids the exposure of other

581   maternal organs to this growth factor. Others reported that *Ascl1* knockdown resulted in

582   an increase in *Igf2* expression in neuronal cells *in vitro* [46]. Thus, this axis may be

583   operating in both maternal hepatocytes and neurons. We gained further insight into this

584   axis in that IGF2 was derived from three placental- and fetal-specific promoters of *Igf2*

585   in maternal hepatocytes without *Ascl1*. How *Ascl1* controls the activities of these three

586   promoters of *Igf2* is another question for the future. We believe that this *Ascl1/Igf2* axis,

587   at least in part, underlies *Ascl1*-dependent phenotypes in the maternal compartment.

588   When maternal hepatocyte *Ascl1* is lost, excess IGF2 is produced in, and elaborated

589   from, these cells. Locally, this promotes maternal hepatocyte proliferation and growth.

590   Systemically, it induces overgrowth of maternal pancreas, spleen, and kidney. Through

591   these autocrine and endocrine pathways, IGF2 partially mediates *Ascl1*-dependent

592   phenotypes. It is highly likely that other maternal organs not examined in this report also

593   respond to the null mutation of maternal hepatic *Ascl1*.

594

595   Our studies demonstrate that *Ascl1* activation in maternal hepatocytes is required

596   to maintain pregnancy-dependent homeostasis of maternal gut microbiota. It is known

597   that the microbiome shows adaptive changes to accommodate the physiological and

598   immunological alterations of the host during pregnancy [25, 47, 48]. Here we found that 8

599   bacteria species in maternal ceca responded to the deficiency of maternal hepatic

600   *Ascl1*. Remarkably, among these bacteria species, *Pseudobutyrivibrio-Roseburia*

601   *intestinalis* was depleted and *Desulfovibrio oxamicus-vulgaris* was aberrantly appeared.

602   The former is known to be associated with the anti-inflammatory activity of colonic

603   mucosa [26], whereas the latter participates in metabolism of various substances such as

604   ammonium, lactate, alcohol, and pyruvate [27]. Therefore, maternal liver, by activating

605   *Ascl1*, controls these two bacteria populations in maternal ceca, revealing new roles for

606   Ascl1 in maternal liver. Several lines of evidence suggest that the other 6 bacteria

607   species are also important to the health of the host [26, 27, 49-52], however, the gestation-

608   dependent functions of these bacteria species remain unclear. Mechanistically, we

609   identified an *Ascl1/Hamp2* axis in maternal hepatocytes as a candidate regulator of

610   maternal gut microbiota. Our data show that *Hamp2* mRNA expression almost fully

611   relies on *Ascl1* activation in maternal hepatocytes. *Hamp2* is produced primarily in the

612   liver, has a strong antimicrobial activity against certain bacteria, and regulates immune

613   responses against bacterial pathogens [53, 54]. Hence, we assume that this *Ascl1/Hamp2*

614   axis in maternal hepatocytes may partially govern the adaptations of maternal gut

615   microbiota to gestation.

616

617   Our studies demonstrate that maternal liver, through activating *Ascl1*, modulates

618   the placenta. This notion is based on our observations that maternal liver *Ascl1*

619   deficiency leads to placenta overgrowth and a change in its function. These phenotypes

620   can be partially interpreted as the consequences of the exposure of the placenta to

621   elevated maternal IGF2. We also observed that hep-*Ascl1*$^{-/-}$ placenta transiently

622   reduced its IGF2 production on gestation day 15 and largely diminished its Erk1/2

623   signaling on gestation day 18 relative to their controls. Thus, the placenta used different

624   mechanisms at distinct stages of pregnancy to defensively respond to increased

625   maternal IGF2, eventually restricting its otherwise further overgrowth. We think that

626   maternal liver activates *Ascl1* to maintain *Igf2* silencing and, by doing this, allows the

627   placenta to appropriately develop and grow without potential maternal inference. It was

628 surprising that the fetal weight was not affected by elevated maternal IGF2. This may

629 suggest that the defense responses of the placenta (reduction in IGF2 production and

630 suppression in Erk1/2 activity) to elevated maternal IGF2 is so strong that the potential

631 stimulatory effect of this potent hormone on fetal growth is fully blocked. However, we

632 did observe severely impaired postnatal growth of the offspring born from hep-*Ascl1*^{-/-}

633 dam. It is a well-established concept that maternal problems generate long-term

634 adverse effects on the health of the next generation [55-57]. Hence, we believe that *Ascl1*

635 deficiency-caused dysregulation of maternal adaptations and placental abnormality

636 together impair the postnatal growth of the offspring. This model warrants further

637 investigations.

638

639 In summary, we demonstrate that, as pregnancy advances, maternal

640 hepatocytes induce expression of *Ascl1* to alter their transcriptomes. Via this

641 mechanism, maternal liver systematically coordinates adaptations in the maternal

642 compartment and allows for optimal placental development and growth, collectively

643 ensuring the health of both the mother and her infant during pregnancy and postnatally.

644

References

646 1. Aagaard K, Riehle K, Ma J, et al. A metagenomic approach to characterization of the vaginal
647 microbiome signature in pregnancy. PLoS One 2012;7:e36466.
648 2. Maymon R, Strauss S, Vaknin Z, et al. Normal sonographic values of maternal spleen size
649 throughout pregnancy. Ultrasound Med Biol 2006;32:1827-31.
650 3. Maymon R, Zimerman AL, Strauss S, et al. Maternal Spleen Size Throughout Normal Pregnancy.
651 Seminars in Ultrasound, CT and MRI 2007;28:64-66.
652 4. Roy C, Saussine C, Jahn C, et al. Fast imaging MR assessment of ureterohydronephrosis during
653 pregnancy. Magn Reson Imaging 1995;13:767-72.
654 5. Beydoun SN. Morphologic changes in the renal tract in pregnancy. Clin Obstet Gynecol
655 1985;28:249-56.

656 6.   Dunlop W. Serial changes in renal haemodynamics during normal human pregnancy. Br J Obstet
657   Gynaecol 1981;88:1-9.
658 7.   Dai G, Bustamante JJ, Zou Y, et al. Maternal hepatic growth response to pregnancy in the
659   mouse. Exp Biol Med (Maywood) 2011;236:1322-32.
660 8.   Ryan JM, Heneghan MA. Pregnancy and the liver. Clinical Liver Disease 2014;4:51-54.
661 9.   Frederiksen MC. Physiologic changes in pregnancy and their effect on drug disposition. Semin
662   Perinatol 2001;25:120-3.
663 10. Guillemot F, Lo LC, Johnson JE, et al. Mammalian achaete-scute homolog 1 is required for the
664   early development of olfactory and autonomic neurons. Cell 1993;75:463-76.
665 11. Casarosa S, Fode C, Guillemot F. Mash1 regulates neurogenesis in the ventral telencephalon.
666   Development 1999;126:525-34.
667 12. Horton S, Meredith A, Richardson JA, et al. Correct coordination of neuronal differentiation
668   events in ventral forebrain requires the bHLH factor MASH1. Mol Cell Neurosci 1999;14:355-69.
669 13. Bustamante JJ, Copple BL, Soares MJ, et al. Gene profiling of maternal hepatic adaptations to
670   pregnancy. Liver International 2010;30:406-415.
671 14. Bertrand N, Castro DS, Guillemot F. Proneural genes and the specification of neural cell types.
672   Nat Rev Neurosci 2002;3:517-30.
673 15. Imayoshi I, Isomura A, Harima Y, et al. Oscillatory control of factors determining multipotency
674   and fate in mouse neural progenitors. Science 2013;342:1203-8.
675 16. Meredith A, Johnson JE. Negative autoregulation of Mash1 expression in CNS development. Dev
676   Biol 2000;222:336-46.
677 17. Altree-Tacha D, Tyrrell J, Li F. mASH1 is Highly Specific for Neuroendocrine Carcinomas: An
678   Immunohistochemical Evaluation on Normal and Various Neoplastic Tissues. Arch Pathol Lab
679   Med 2017;141:288-292.
680 18. Andersen J, Urbán N, Achimastou A, et al. A transcriptional mechanism integrating inputs from
681   extracellular signals to activate hippocampal stem cells. Neuron 2014;83:1085-1097.
682 19. Truett GE, Heeger P, Mynatt RL, et al. Preparation of PCR-quality mouse genomic DNA with hot
683   sodium hydroxide and tris (HotSHOT). Biotechniques 2000;29:52, 54.
684 20. Pacary E, Heng J, Azzarelli R, et al. Proneural Transcription Factors Regulate Different Steps of
685   Cortical Neuron Migration through Rnd-Mediated Inhibition of RhoA Signaling. Neuron
686   2011;69:1069-1084.
687 21. Schneider CA, Rasband WS, Eliceiri KW. NIH Image to ImageJ: 25 years of image analysis. Nat
688   Methods 2012;9:671-5.
689 22. Yang P, Wang Y, Hoang D, et al. A placental growth factor is silenced in mouse embryos by the
690   zinc finger protein ZFP568. Science 2017;356:757-759.
691 23. Yanger K, Zong Y, Maggs LR, et al. Robust cellular reprogramming occurs spontaneously during
692   liver regeneration. Genes Dev 2013;27:719-24.
693 24. Ho KJ, Bass CE, Kroemer AH, et al. Optimized adeno-associated virus 8 produces hepatocyte-
694   specific Cre-mediated recombination without toxicity or affecting liver regeneration. Am J
695   Physiol Gastrointest Liver Physiol 2008;295:G412-9.
696 25. Koren O, Goodrich JK, Cullender TC, et al. Host remodeling of the gut microbiome and metabolic
697   changes during pregnancy. Cell 2012;150:470-80.
698 26. Zhu C, Song K, Shen Z, et al. Roseburia intestinalis inhibits interleukin-17 excretion and promotes
699   regulatory T cells differentiation in colitis. Molecular medicine reports 2018;17:7567-7574.
700 27. López-Cortés A, Fardeau M-L, Fauque G, et al. Reclassification of the sulfate- and nitrate-
701   reducing bacterium Desulfovibrio vulgaris subsp. oxamicus as Desulfovibrio oxamicus sp. nov.,
702   comb. nov. International Journal of Systematic and Evolutionary Microbiology 2006;56:1495-
703   1499.

28. Liu ZM, Chen J, Lv YP, et al. Molecular characterization of a hepcidin homologue in starry flounder (Platichthys stellatus) and its synergistic interaction with antibiotics. Fish Shellfish Immunol 2018;83:45-51.

29. Gui L, Zhang P, Zhang Q, et al. Two hepcidins from spotted scat (Scatophagus argus) possess antibacterial and antiviral functions in vitro. Fish Shellfish Immunol 2016;50:191-9.

30. Simmons DG, Rawn S, Davies A, et al. Spatial and temporal expression of the 23 murine Prolactin/Placental Lactogen-related genes is not associated with their position in the locus. BMC Genomics 2008;9:352.

31. Bergman D, Halje M, Nordin M, et al. Insulin-like growth factor 2 in development and disease: a mini-review. Gerontology 2013;59:240-9.

32. Constancia M, Hemberger M, Hughes J, et al. Placental-specific IGF-II is a major modulator of placental and fetal growth. Nature 2002;417:945-8.

33. Sferruzzi-Perri AN, Sandovici I, Constancia M, et al. Placental phenotype and the insulin-like growth factors: resource allocation to fetal growth. J Physiol 2017;595:5057-5093.

34. Soares MJ. The prolactin and growth hormone families: pregnancy-specific hormones/cytokines at the maternal-fetal interface. Reproductive biology and endocrinology : RB&E 2004;2:51-51.

35. Campbell WJ, Larsen D, Deb S, et al. Expression of alkaline phosphatase in differentiated rat labyrinthine trophoblast tissue. Placenta 1991;12:227-37.

36. Kent LN, Ohboshi S, Soares MJ. Akt1 and insulin-like growth factor 2 (Igf2) regulate placentation and fetal/postnatal development. The International journal of developmental biology 2012;56:255-261.

37. Kuida K, Boucher DM. Functions of MAP kinases: insights from gene-targeting studies. J Biochem 2004;135:653-6.

38. Rotwein P, Hall LJ. Evolution of Insulin-Like Growth Factor II: Characterization of the Mouse IGF-II Gene and Identification of Two Pseudo-Exons. DNA and Cell Biology 1990;9:725-735.

39. Tabata H, Kobayashi M, Ikeda JH, et al. Characterization of multiple first exons in murine prolactin receptor gene and the effect of prolactin on their expression in the choroid plexus. J Mol Endocrinol 2012;48:169-76.

40. Lu L, Li Y, Kim SM, et al. Hippo signaling is a potent in vivo growth and tumor suppressor pathway in the mammalian liver. Proceedings of the National Academy of Sciences of the United States of America 2010;107:1437-1442.

41. Brouwer-Visser J, Huang GS. IGF2 signaling and regulation in cancer. Cytokine & Growth Factor Reviews 2015;26:371-377.

42. Liu J, Hu X, Chen J, et al. Pericentral hepatocytes produce insulin-like growth factor-2 to promote liver regeneration during selected injuries in mice. Hepatology 2017;66:2002-2015.

43. Pattyn A, Simplicio N, van Doorninck JH, et al. Ascl1/Mash1 is required for the development of central serotonergic neurons. Nat Neurosci 2004;7:589-95.

44. Peltopuro P, Kala K, Partanen J. Distinct requirements for Ascl1 in subpopulations of midbrain GABAergic neurons. Dev Biol 2010;343:63-70.

45. Chanda S, Ang CE, Davila J, et al. Generation of induced neuronal cells by the single reprogramming factor ASCL1. Stem Cell Reports 2014;3:282-96.

46. Li J, Neumann I, Volkmer I, et al. Down-regulation of achaete-scute complex homolog 1 (ASCL1) in neuroblastoma cells induces up-regulation of insulin-like growth factor 2 (IGF2). Molecular Biology Reports 2011;38:1515-1521.

47. Konstantinov SR, van der Woude CJ, Peppelenbosch MP. Do pregnancy-related changes in the microbiome stimulate innate immunity? Trends Mol Med 2013;19:454-9.

48. Mulligan CM, Friedman JE. Maternal modifiers of the infant gut microbiota: metabolic consequences. J Endocrinol 2017;235:R1-R12.

752 49. Fox JG, Dewhirst FE, Tully JG, et al. Helicobacter hepaticus sp. nov., a microaerophilic bacterium
753   isolated from livers and intestinal mucosal scrapings from mice. J Clin Microbiol 1994;32:1238-
754   45.
755 50. Yang JY, Lee YS, Kim Y, et al. Gut commensal Bacteroides acidifaciens prevents obesity and
756   improves insulin sensitivity in mice. Mucosal Immunol 2017;10:104-116.
757 51. Kanauchi O, Fujiyama Y, Mitsuyama K, et al. Increased growth of Bifidobacterium and
758   Eubacterium by germinated barley foodstuff, accompanied by enhanced butyrate production in
759   healthy volunteers. Int J Mol Med 1999;3:175-9.
760 52. Bereswill S, Ekmekciu I, Escher U, et al. Lactobacillus johnsonii ameliorates intestinal, extra-
761   intestinal and systemic pro-inflammatory immune responses following murine Campylobacter
762   jejuni infection. Scientific reports 2017;7:2138-2138.
763 53. Lu S, Seravalli J, Harrison-Findik D. Inductively coupled mass spectrometry analysis of biometals
764   in conditional Hamp1 and Hamp1 and Hamp2 transgenic mouse models. Transgenic research
765   2015;24:765-773.
766 54. Pigeon C, Ilyin G, Courselaud B, et al. A new mouse liver-specific gene, encoding a protein
767   homologous to human antimicrobial peptide hepcidin, is overexpressed during iron overload. J
768   Biol Chem 2001;276:7811-9.
769 55. Catalano PM, Shankar K. Obesity and pregnancy: mechanisms of short term and long term
770   adverse consequences for mother and child. BMJ (Clinical research ed.) 2017;356:j1-j1.
771 56. Dunlop AL, Mulle JG, Ferranti EP, et al. Maternal Microbiome and Pregnancy Outcomes That
772   Impact Infant Health: A Review. Adv Neonatal Care 2015;15:377-85.
773 57. Chen X, Zhao D, Mao X, et al. Maternal Dietary Patterns and Pregnancy Outcome. Nutrients
774   2016;8:351.

775

A

B
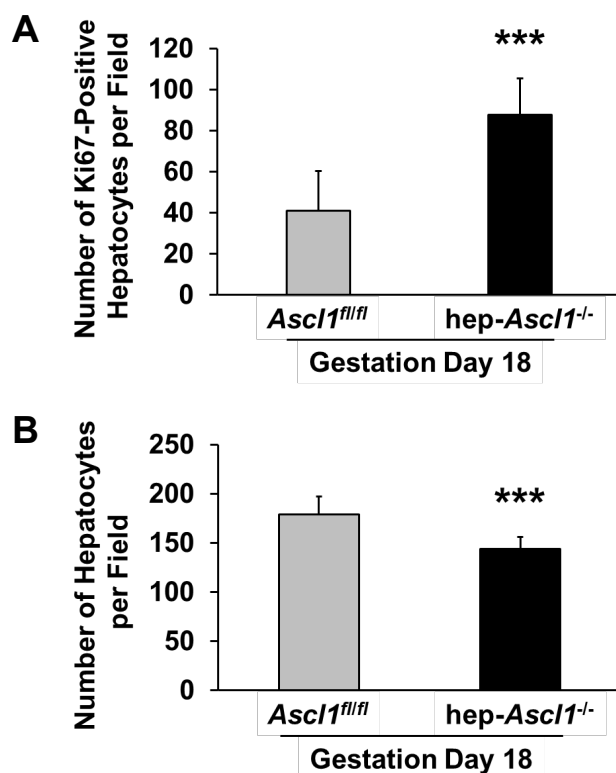
Supplemental Fig. 1. Maternal hepatocyte-specific *Ascl1* knockout results in increased maternal hepatocyte proliferation and hypertrophy. Livers were collected from nonpregnant (NP) and gestation day (GD) 18 *Ascl1*$^{fl/fl}$ and hep-*Ascl1*$^{-/-}$ mice. Liver sections were subjected to **(A)** Ki67 and **(B)** β-Catenin staining. Ki67- and β-Catenin-positive hepatocytes were counted in five random fields of view (X200 magnification) and presented as the means ± SD (n = 3-6 and n=7 for each group, respectively). ***, $P < 0.001$, between *Ascl1*$^{fl/fl}$ and hep-*Ascl1*$^{-/-}$ mice.
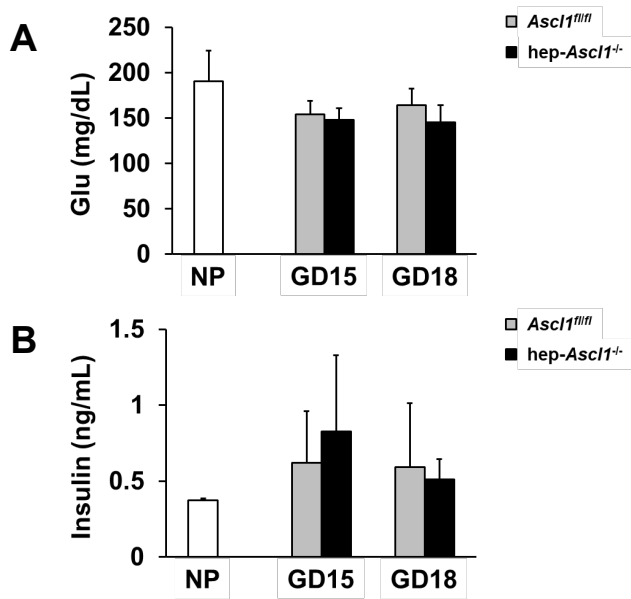
Supplemental Fig. 2. Maternal hepatocyte-specific *Ascl1* knockout does not affect the concentrations of glucose and insulin in maternal blood. Serums were collected from nonpregnant (NP) and gestation days (GD) 15 and 18 *Ascl1*^{fl/fl} and hep-*Ascl1*^{-/-} mice. Serum **(A)** glucose and **(B)** insulin are presented as means ± SD (n = 3-6). *Ascl1*, achaete-scute homolog 1; Glu, glucose.
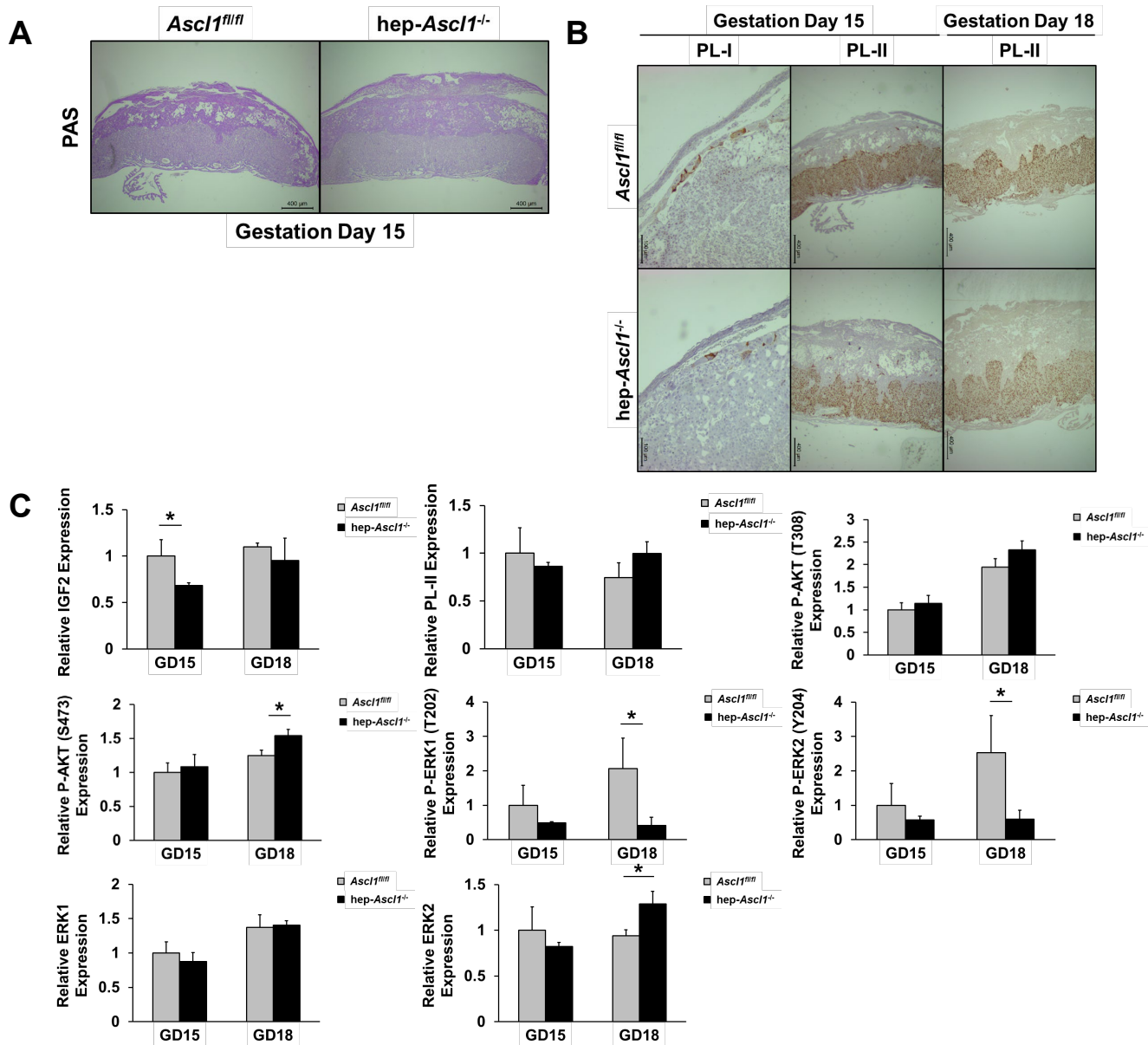
Supplemental Fig. 3. Maternal hepatocyte-specific *Ascl1* knockout partially influences placental function. Placentas were collected from gestation days (GD) 15 and 18 *Ascl1^fl/fl^* and hep-*Ascl1^-/-^* mice. **(A)** Frozen placental sections underwent periodic acid-Schiff (PAS) staining. Glycogen is stained red to purple. **(B)** Frozen placental sections were subjected to *PL-I* and *PL-II in situ* hybridization staining using RNAscope 2.5 HD Assay-BROWN kit. The *PL-I* and *PL-II* mRNAs are stained dark brown. **(C)** Quantification of relative intensity of Western blotting signals from **Figure 6D**. Data are presented as the mean fold changes relative to GD15 *Ascl1^fl/fl^* mice (± SD; n = 3 for each group). *, $P < 0.05$, between *Ascl1^fl/fl^* and hep-*Ascl1^-/-^* mice. AKT, total protein kinase B; *Ascl1*, achaete-scute homolog 1; ERK1/2, extracellular signal-regulated kinase 1/2; GAPDH, glyceraldehyde 3-phosphate dehydrogenase; IGF2, insulin-like growth factor; PL-II, placental lactogen II.
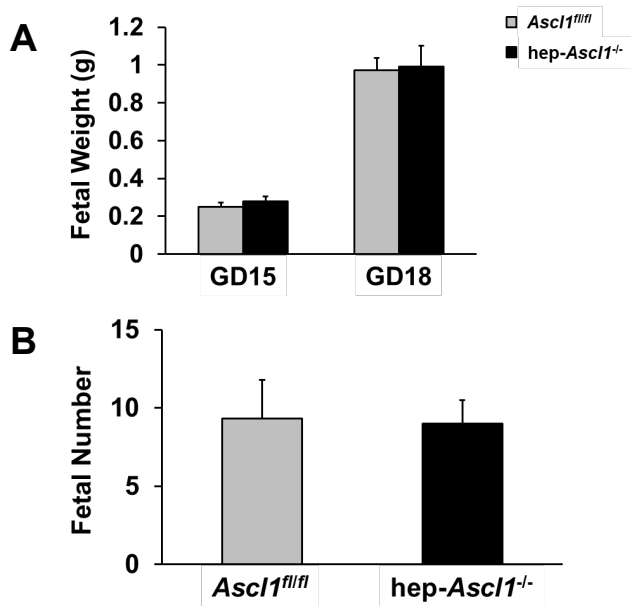
Supplemental Fig. 4. Maternal hepatocyte-specific *Ascl1* knockout does not affect fetal weight and numbers. Fetuses were weighed from gestation days (GD) 15 and 18 *Ascl1^{fl/fl}* and hep-*Ascl1^{-/-}* mice. **(A)** Fetal weight and **(B)** numbers are presented as means ± SD (n = 13-31). *Ascl1*, achaete-scute homolog 1.

Primer Name	Primer Type	Sequence 5' -> 3'
Ascl1 Forward	Common Forward	CTA CTG TCC AAA CGC AAA GTG G
Ascl1 Wildtype Reverse	Wildtype Reverse	GCT CCC ACA ATC CTC GTA AAG A
Ascl1 Mutant Reverse	Mutant Reverse	TAG ACG TTG TGG CTG TTG TAG T

Gene	Assay ID	Catalog No.
Ascl1	Mm03058063_m1	4453320
Igf2	Mm00439564_m1	4331182
Hamp2	Mm00842044_g1	4331182
18S	Mm03928990_g1	4453320

Primer Name	Sequence 5' -> 3'
Igf2-all_F	CGG CTT CTA CTT CAG CAG GC
Igf2-all_R	GTA TCT GGG GAA GTC GTC CG
Igf2-P0_F	TTT ATC CAC CGT CCG GGA AC
Igf2-P0_R	GCA GTC GTC GTA GTC GTT CT
Igf2-P1_F	CGG CAG CAC AGA TTT TGG AA
Igf2-P1_R	CAC CAA CAT CGA CTT CCC CA
Igf2-P2_F	CCC CAG CCC TAA GAT ACC CTA A
Igf2-P2_R	AGC ACC AAC ATC GAC TTC CC
Igf2-P3_F	CGG CCT CCT TAC CCA ACT TC
Igf2-P3_R	GGG GTG GCA CAG TAT GTC TC
18S_F	CTC AAC ACG GGA AAC CTC AC
18S_R	CGC TCC ACC AAC TAA GAA CG